

The α effect with imposed and dynamo-generated magnetic fields

A. Hubbard,^{1*} F. Del Sordo,^{1,2} P. J. Käpylä³ and A. Brandenburg^{1,2}

¹*NORDITA, AlbaNova University Center, Roslagstullsbacken 23, SE-10691 Stockholm, Sweden*

²*Department of Astronomy, Alba Nova University Center, Stockholm University, SE-10691 Stockholm, Sweden*

³*Observatory Tähtitorninmäki, PO Box 14, University of Helsinki, FI-00014 Helsinki, Finland*

Accepted 2009 May 12. Received 2009 May 12; in original form 2009 April 20

ABSTRACT

Estimates for the non-linear α effect in helical turbulence with an applied magnetic field are presented using two different approaches: the imposed-field method where the electromotive force owing to the applied field is used, and the test-field method where separate evolution equations are solved for a set of different test fields. Both approaches agree for stronger fields, but there are apparent discrepancies for weaker fields that can be explained by the influence of dynamo-generated magnetic fields on the scale of the domain that are referred to as meso-scale magnetic fields. Examples are discussed where these meso-scale fields can lead to both drastically overestimated and underestimated values of α compared with the kinematic case. It is demonstrated that the kinematic value can be recovered by resetting the fluctuating magnetic field to zero in regular time intervals. It is concluded that this is the preferred technique both for the imposed-field and the test-field methods.

Key words: hydrodynamics – magnetic fields – MHD – turbulence.

1 INTRODUCTION

The α effect is commonly used to describe the evolution of the large-scale magnetic field in hydromagnetic dynamos (Moffatt 1978; Parker 1979; Krause & Rädler 1980). However, the α effect is not the only known mechanism for explaining the generation of large-scale magnetic fields. Two more effects have been discussed in cases when there is shear in the system: the incoherent alpha-shear dynamo (Vishniac & Brandenburg 1997; Sokolov 1997; Silant'ev 2000; Proctor 2007) and the shear-current effect (Rogachevskii & Kleeorin 2003, 2004). In order to provide some understanding of the magnetic field generation in astrophysical bodies such as the Sun or the Galaxy, or at least in numerical simulations of these systems, it is of interest to be able to identify the underlying mechanism.

Astrophysical dynamos are usually confined to finite domains harbouring turbulent fluid motion. Both the Sun and the Galaxy are gravitationally stratified and rotating, which makes the turbulence non-mirror symmetric, thus leading to an α effect. In addition, the rotation is non-uniform, which leads to a strong amplification of the magnetic field in the toroidal direction, as well as other effects such as those mentioned above. Instead of simulating such systems with all their ingredients, it is useful to simplify the set-up by restricting oneself to Cartesian domains that can be thought to represent a part of the full domain. At low magnetic Reynolds numbers, i.e. when the effects of induction are comparable to those of magnetic diffusion, the α effect can clearly be identified in simulations of convection in Cartesian domains; see Brandenburg et al.

(1990). Here, α has been determined by applying a uniform magnetic field across the simulation domain and measuring the resulting electromotive force. This method is referred to as the imposed-field method. However, in subsequent years simulations at larger magnetic Reynolds numbers have revealed problems in that the resulting α becomes smaller and strongly fluctuating in time. This was first found in simulations where the turbulence is caused by an externally imposed body force (Cattaneo & Hughes 1996; Hughes & Cattaneo 2008), but it was later also found for convection (Cattaneo & Hughes 2006). This suggested that the mean-field approach may be seriously flawed (Cattaneo & Hughes 2009).

Meanwhile, there have been a number of simulations of convection where large-scale magnetic fields are being generated. Such systems include simulations not only in spherical shells (Browning et al. 2006; Brown et al. 2007), but also in Cartesian domains (Käpylä, Korpi & Brandenburg 2008, 2009a; Hughes & Proctor 2009). However, the absence of a significant α effect in some of these simulations led Hughes & Proctor (2009) to the conclusion that such magnetic fields can only be explained by other mechanisms such as the incoherent alpha-shear dynamo or the shear-current effect. Such an explanation seems to be in conflict with earlier claims of a finite α effect as determined by the test-field method of Schrunner et al. (2005, 2007), and in particular with recent results for convection (Käpylä, Korpi & Brandenburg 2009b). The purpose of the present paper is therefore to discuss possible reasons for conflicting results that are based on different methods. The idea is to compare measurements of the α effect using both the imposed-field method and the test-field method. We consider here the case of helically forced turbulence in a triply periodic domain. This case is believed to be well understood. We expect

*E-mail: hubbard@pas.rochester.edu

α to be catastrophically quenched, i.e. α is suppressed for field strengths exceeding the Zeldovich (1957) value of $R_m^{-1/2} B_{\text{eq}}$, where B_{eq} is the equipartition field strength where kinetic and magnetic energy densities are comparable. The importance of the Zeldovich field strength was emphasized by Gruzinov & Diamond (1994) in connection with catastrophic quenching resulting from magnetic helicity conservation.

In this paper we focus on the case of moderate values of R_m of around 30. This is small by comparison with astrophysical applications, but it is large compared with the critical value for dynamo action in fully helical turbulence (Brandenburg 2001), which occurs for $R_m \gtrsim 1$ in our definition of R_m based on the wavenumber of the scale of the energy carrying eddies, i.e. the forcing wavenumber. In addition, we only consider cases with a magnetic Prandtl number of unity. However, this should not worry us too much, because we know that the large-scale dynamo works independently of the value of the magnetic Prandtl number (Mininni 2007; Brandenburg 2009).

2 HELICAL TURBULENCE AND α EFFECT

2.1 Forced turbulence simulations

Throughout this paper we consider hydromagnetic turbulence in the presence of a mean magnetic field \mathbf{B}_0 using triply periodic boundary conditions. The total magnetic field is written as $\mathbf{B}_0 + \nabla \times \mathbf{A}$, where \mathbf{A} is the magnetic vector potential. We employ an isothermal equation of state where the pressure is proportional to the density, $p = \rho c_s^2$, with c_s being the isothermal sound speed. The governing evolution equations for logarithmic density $\ln \rho$, velocity \mathbf{U} , together with \mathbf{A} , are given by

$$\frac{d \ln \rho}{dt} = -\nabla \cdot \mathbf{U}, \quad (1)$$

$$\frac{d\mathbf{U}}{dt} = \mathbf{J} \times (\mathbf{B}_0 + \mathbf{B})/\rho + \mathbf{f} + \mathbf{F}_{\text{visc}} - c_s^2 \nabla \ln \rho, \quad (2)$$

$$\frac{\partial \mathbf{A}}{\partial t} = \mathbf{U} \times (\mathbf{B}_0 + \mathbf{B}) + \eta \nabla^2 \mathbf{A}, \quad (3)$$

where $\mathbf{B}_0 + \mathbf{B}$ is the total magnetic field, but since $\mathbf{B}_0 = \text{const}$ it does not enter in the mean current density, which is given by $\mathbf{J} = \nabla \times \mathbf{B}/\mu_0$, where μ_0 is the vacuum permeability. Furthermore, $d/dt = \partial/\partial t + \mathbf{U} \cdot \nabla$ is the advective derivative, $\mathbf{F}_{\text{visc}} = \rho^{-1} \nabla \cdot 2\rho\nu\mathbf{S}$ is the viscous force, ν is the kinematic viscosity, $\mathbf{S}_{ij} = (1/2)(U_{i,j} + U_{j,i}) - (1/3)\delta_{ij} \nabla \cdot \mathbf{U}$ is the traceless rate of strain tensor and \mathbf{f} is a random forcing function consisting of plane transversal waves with random wavevectors \mathbf{k} such that $|\mathbf{k}|$ lies in a band around a given forcing wavenumber k_f . The vector \mathbf{k} changes randomly from one time-step to the next. This method is described for example in Haugen, Brandenburg & Dobler (2004). The forcing amplitude is chosen so that the Mach number $\text{Ma} = u_{\text{rms}}/c_s$ is about 0.1.

We consider a domain of size $L_x \times L_y \times L_z$. We use $L_x = L_y = L_z = 2\pi/k_1$ in all cases. Our model is characterized by the choice of magnetic Reynolds and Prandtl numbers, defined here via

$$R_m = u_{\text{rms}}/\eta k_f, \quad P_m = \nu/\eta. \quad (4)$$

We start the simulations with zero initial magnetic field, so the field is entirely produced by the imposed field. The value of the magnetic field will be expressed in units of the equipartition value

$$B_{\text{eq}} = \langle \mu_0 \rho \mathbf{u}^2 \rangle^{1/2}. \quad (5)$$

We consider values of B_0/B_{eq} from 0.06 to 20 along with a magnetic Reynolds number of about 26, adequate to support dynamo action.

2.2 α from the imposed-field method

The present simulations allow us to determine directly the α effect under the assumption that the relevant mean field is given by volume averages, denoted here by angular brackets. Given that the magnetic field is written as $\mathbf{B} = \nabla \times \mathbf{A}$ where \mathbf{A} is also triply periodic, we have $\langle \mathbf{B} \rangle = \mathbf{0}$. We can determine the volume-averaged electromotive force:

$$\langle \mathcal{E} \rangle = \langle \mathcal{E} \rangle(t) \equiv \langle \mathbf{u} \times \mathbf{b} \rangle, \quad (6)$$

where $\mathbf{u} = \mathbf{U} - \langle \mathbf{U} \rangle$ and $\mathbf{b} = \mathbf{B}$ are the fluctuating components of velocity and magnetic field, and $\langle \mathbf{B} \rangle = \langle \nabla \times \mathbf{A} \rangle = \mathbf{0}$.

For mean fields defined as volume averages, and because of periodic boundary conditions, we have $\langle \mathbf{J} \rangle = \mathbf{0}$. Under isotropic conditions there is therefore only the α effect connecting $\langle \mathcal{E} \rangle$ with \mathbf{B}_0 via $\langle \mathcal{E} \rangle = \alpha_{\text{imp}} \mathbf{B}_0$, so

$$\alpha_{\text{imp}} = \langle \mathcal{E} \rangle \cdot \mathbf{B}_0 / B_0^2. \quad (7)$$

In all cases reported below we assume $\mathbf{B}_0 = (B_0, 0, 0)$. Note that $\nabla \times \langle \mathcal{E} \rangle = \mathbf{0}$ and therefore our time-constant imposed field is self-consistent.

2.3 α from the test-field method

A favoured method of determining the full α_{ij} tensor is by using the test-field method (Schrinner et al. 2005, 2007), where one solves, in addition to equations (1)–(3), a set of equations. In the special case of volume averages this set of equations simplifies to

$$\frac{\partial \mathbf{a}^q}{\partial t} = \overline{\mathbf{U}} \times \mathbf{b}^q + \mathbf{u} \times (\mathbf{B}_0 + \overline{\mathbf{B}}^q) + \mathbf{u} \times \mathbf{b}^q - \overline{\mathbf{u} \times \mathbf{b}^q} + \eta \nabla^2 \mathbf{a}^q, \quad (8)$$

where $\mathbf{b}^q = \nabla \times \mathbf{a}^q$ with $q = 1$ or 2 denotes the response to each of the two test fields $\overline{\mathbf{B}}^q$. Throughout this paper, overbars denote planar averages. Later we consider arbitrary planar averages and denote their normals by superscripts, but here we restrict ourselves to xy averages. We use two different constant test fields:

$$\overline{\mathbf{B}}^1 = (\mathcal{B}, 0, 0), \quad \overline{\mathbf{B}}^2 = (0, \mathcal{B}, 0), \quad (9)$$

where $\mathcal{B} = \text{const}$ is the magnitude of the test field, but its actual value is of no direct significance, because the \mathcal{B} factor cancels in the calculation of α .

However, given that the test-field equations are linear in \mathbf{b}^q , this field can grow exponentially due to dynamo action. When $|\mathbf{b}^q|$ becomes larger than about 20 times the value of \mathcal{B} , the determination of α becomes increasingly inaccurate, so it is advisable to reset \mathbf{b}^q to zero in regular intervals (Sur, Brandenburg & Subramanian 2008). We calculate the corresponding values of the electromotive force $\langle \mathcal{E} \rangle^q = \langle \mathbf{u} \times \mathbf{b}^q \rangle$ to determine the components

$$\alpha_{iq} = \langle \mathcal{E} \rangle_i^q / \mathcal{B}. \quad (10)$$

This corresponds to the special case $k = 0$ when considering sinusoidal and cosinusoidal test functions described elsewhere (Brandenburg, Rädler & Schrinner 2008a).

Even though the test-field equations themselves are linear, the flow field is affected by the actual magnetic field (which is different from the test field), so the resulting α tensor is being affected

(‘quenched’) by the magnetic field. This was successfully demonstrated in Brandenburg et al. (2008b), where α_{ij} takes the form

$$\alpha_{ij} = \alpha_1 \delta_{ij} + \alpha_2 \hat{B}_i \hat{B}_j. \quad (11)$$

Here $\hat{B} = \bar{\mathbf{B}}/|\bar{\mathbf{B}}|$ is the unit vector of the relevant mean magnetic field. In the induction equation the α effect occurs only in the combination

$$\alpha_{ij} \bar{B}_j = (\alpha_1 + \alpha_2) \bar{B}_i, \quad (12)$$

and this is also what is determined by the imposed-field method, but it is different from the mean values of the components of the α_{ij} tensor. On the other hand, in the case of a passive vector field it is the mean components of α_{ij} rather than the components of $\alpha_{ij} \bar{B}_j$ that are of immediate importance (Tilgner & Brandenburg 2008).

2.4 α in the presence of meso-scale fields

The *relevant* mean field may not just be the imposed field with wavenumber $k = 0$, but it may well be a field with wavenumber $k = k_1$. Such a field would vanish under volume averaging, but it would still produce finite values of $\langle \hat{B}_i \hat{B}_j \rangle$. For the diagonal components of $\langle \alpha_{ij} \rangle$ we can write

$$\langle \alpha_{xx} \rangle = \alpha_1 + \epsilon_x \alpha_2, \quad \langle \alpha_{yy} \rangle = \alpha_1 + \epsilon_y \alpha_2, \quad (13)$$

where the factors

$$\epsilon_x = \langle \hat{B}_x^2 \rangle \quad \text{and} \quad \epsilon_y = \langle \hat{B}_y^2 \rangle \quad (14)$$

quantify the weight of the α_2 term. For a purely uniform field pointing in the x direction we have $\epsilon_x = 1$ and $\epsilon_y = 0$, while for a Beltrami field of the form $\bar{\mathbf{B}} = (\cos kz, \sin kz, 0)$ we have $\epsilon_x = \epsilon_y = 1/2$.

In practice we will have a mixture between the imposed field (below sometimes referred to as large-scale field) and a dynamo-generated magnetic field with typical wavenumber $k = k_1$ (below sometimes referred to as meso-scale magnetic field). The solution to the test-field equations, \mathbf{b}^q , can also develop meso-scale fields with wavevectors in the x or y directions, but not in the z direction, because that component is removed by the term $\mathbf{u} \times \mathbf{b}^q$ in equation (8). Table 1 highlights the difference between imposed, meso-scale and test fields. We denote the ratio of the strengths of imposed and meso-scale fields as $\beta = B_0/B_1$ and distinguish three (and later four) different cases, depending on the direction of the wavevector of the Beltrami field.

The first case is referred to as the X branch, because the wavevector of the Beltrami field points in the x direction. To calculate ϵ_x there is, in addition to the imposed field B_0 , a Beltrami field $B_1(0, \cos kx, \sin kx)$, which does not have a component in the x direction. Thus, $B_x = B_0$, and since $\mathbf{B} = (B_0, B_1 \cos kx, B_1 \sin kx)$, we have $B^2 = B_0^2 + B_1^2$, so $\epsilon_x = \hat{B}_x^2 = B_0^2/(B_0^2 + B_1^2)$, or $\epsilon_x = \beta^2/(1 + \beta^2)$. Likewise, with $B_y = B_1 \cos kx$ we find for the volume average or, in this case, the x average $\langle B_y^2 \rangle = B_1^2/2$, so $\epsilon_y = 1/[2(1 + \beta^2)]$.

The next case is referred to as the Y branch, because the wavevector of the Beltrami field points in the y direction. Thus, we have

Table 1. Overview of the different types of fields and their meaning.

Field	Symbol	Magn	Induct. eqn	Test-field eqn
Imposed field	B_0	B_0	Yes	Yes
Meso-scale field	$\bar{\mathbf{B}}$	B_1	Yes	–
Test field	$\bar{\mathbf{B}}^q$	B	–	Yes
Test field response	\mathbf{b}^q	–	–	Yes

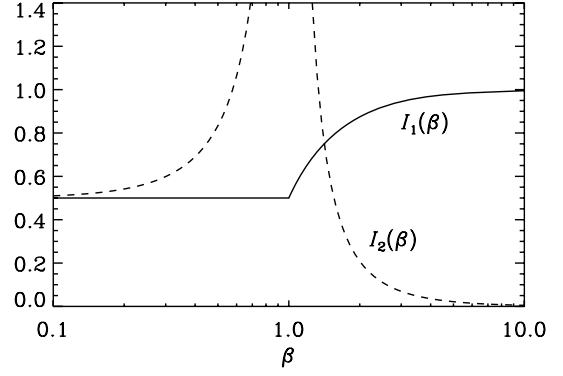


Figure 1. Plot of the integrals $I_1(\beta)$ and $I_2(\beta)$.

$\mathbf{B} = (B_0 + B_1 \sin ky, 0, B_1 \cos ky)$, so $B^2 = B_0^2 + 2B_0 B_1 \sin ky + B_1^2$. This is no longer independent of position, so the volume average or, in this case, the y average has to be obtained by integration. Thus, we write $\epsilon_x = I_1(\beta)$ where we have defined

$$I_1(\beta) = \int_0^{2\pi} \frac{(\beta + \sin \theta)^2}{\beta^2 + 2\beta \sin \theta + 1} d\theta = \begin{cases} 1/2 & \beta^2 \leq 1, \\ 1 - 1/2\beta^2 & \beta^2 > 1, \end{cases}$$

where $\theta = ky$ has been introduced as dummy variable. Since $B_y = 0$ in this case, we have $\epsilon_y = 0$.

Finally, for the Z branch, where the wavevector of the Beltrami field points in the z direction, we have $\mathbf{B} = (B_0 + B_1 \cos kz, B_1 \sin kz, 0)$, we find $\epsilon_x = I_1(\beta)$ and $\epsilon_y = I_2(\beta)$ with

$$I_2(\beta) = \int_0^{2\pi} \frac{\cos^2 \theta}{\beta^2 + 2\beta \cos \theta + 1} \frac{d\theta}{2\pi} = \begin{cases} I_0(\beta) & \beta^2 < 1, \\ I_0(\beta)/\beta^2 & \beta^2 > 1, \end{cases}$$

where $I_0(\beta) = (1 + \beta^2)/[2(1 - \beta^2)]$ and $\theta = kz$ has been used as a dummy variable. A graphical representation of the integrals is given in Fig. 1 and a summary of the expressions for $\epsilon_x(\beta)$ and $\epsilon_y(\beta)$ as well as $\epsilon_x(0)$ and $\epsilon_y(0)$ for the X, Y and Z branches is given in Table 2. The singularity in $I_0(\beta)$ could potentially affect α_{yy} . However, the results shown below show that, at least for stronger fields, α_2 goes to zero near the singularity of $I_0(\beta)$ such that α_{yy} remains finite.

3 RESULTS

We have performed simulations for values of B_0 in the range $0.06 \leq R_m^{1/2} B_0/B_{\text{eq}} \leq 20$ for $R_m \approx 26$ and $P_m = 1$. In all cases we use $k_f/k_1 = 3$, which is big enough to allow a meso-scale magnetic field of wavenumber k_1 to develop within the domain; see Fig. 2. We did not initially anticipate the importance of the meso-scale fields. Different runs were found to exhibit rather different behaviour which turned out to be related to their random positioning on different branches. We used the existing results from different branches as initial conditions for neighbouring values of B_0 .

In this paper, error bars are estimated from the averages obtained from any of three equally long subsections of the full time series.

Table 2. Summary of the expressions for $\epsilon_x(\beta)$ and $\epsilon_y(\beta)$ as well as $\epsilon_x(0)$ and $\epsilon_y(0)$ for the X, Y and Z branches.

Branch	$\epsilon_x(\beta)$	$\epsilon_y(\beta)$	$\epsilon_x(0)$	$\epsilon_y(0)$
X	$\beta^2/(1 + \beta^2)$	$1/[2(1 + \beta^2)]$	0	1/2
Y	$I_1(\beta)$	0	1/2	0
Z	$I_1(\beta)$	$I_2(\beta)$	1/2	1/2

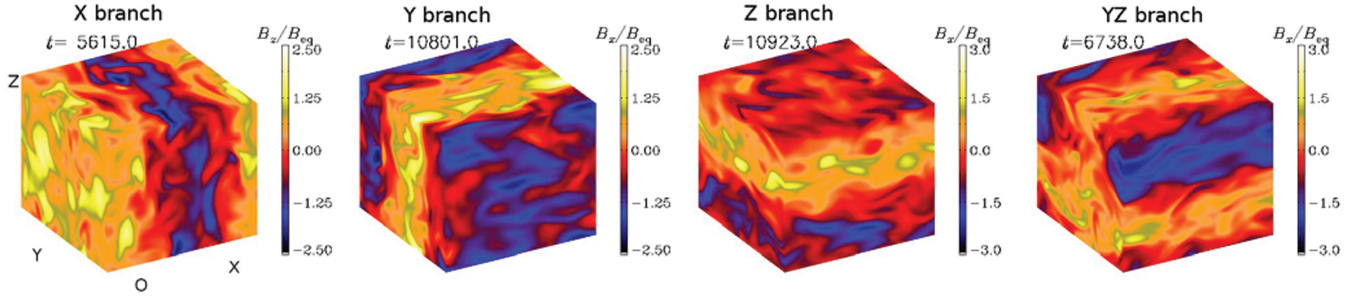


Figure 2. Visualization of B_z on the periphery of the computational domain for the X branch and B_x for the Y, Z and YZ branches. The coordinate directions are indicated on the first panel.

The error bars are comparable with the typical scatter of the data points, but they are not shown because they would make the figure harder to read. Note that the results in this section consider saturated fields. The opposite case will be considered in Section 4.

3.1 Different branches

The resulting values of α are shown in Fig. 3. For strong imposed magnetic fields, $R_m \mathbf{B}_0^2 / B_{\text{eq}}^2 > 1$, the resulting dependence of α on B_0 obeys the standard catastrophic quenching formula for the case of a uniform magnetic field (Vainshtein & Cattaneo 1992):

$$\alpha_{\text{fit}} = \frac{\alpha_0}{1 + \tilde{R}_m \mathbf{B}^2 / B_{\text{eq}}^2} \quad (\text{for } \overline{\mathbf{B}} = \mathbf{B}_0 = \text{const only}), \quad (15)$$

where $\alpha_0 = -(1/3) u_{\text{rms}}$ is the relevant kinematic reference value for fully helical turbulence with negative helicity and $R_m > 1$ (Sur et al. 2008). We treat \tilde{R}_m as an empirical fit parameter that is proportional to R_m and find that $\tilde{R}_m / R_m \approx 0.4$ gives a reasonably good fit; see the dash-dotted line in Fig. 3. The existence of such an empirical factor might be related to fact that the relevant quantity could be the width of the magnetic inertial range, and that this is not precisely equal to R_m . For $R_m \mathbf{B}_0^2 / B_{\text{eq}}^2 > 1$, a similar result is also reproduced using the test-field method, although α_{xx} is typically somewhat larger than α_{imp} .

For weak imposed magnetic fields, $R_m \mathbf{B}_0^2 / B_{\text{eq}}^2 < 1$, apparent discrepancies are found between the imposed-field method and the test-field method. In fact, in the graphical representation in Fig. 3 the results can be subdivided into four different branches that we refer to as branches X, Y, Z and YZ. These names have to do with the orientation of a dynamo-generated magnetic field. These dynamo-generated magnetic fields take the form of Beltrami fields that vary in the x , y and z directions for branches X, Y and Z, while for branch YZ the field varies both in the y and z directions. Earlier work without imposed fields has shown that branch YZ can be accessed during intermediate times during the saturation of the dynamo, but it is not one of the ultimate stable branches X, Y or Z.

Branches Y and Z show the sudden onset of suppression of α_{imp} for *weak* magnetic fields. This has to do with the fact that for weak imposed magnetic fields a dynamo-generated field of Beltrami type is being generated. Such fields quench the α effect, even though they do not contribute to the volume-averaged mean field. On branch YZ the α effect is only weakly suppressed, while on branch X the imposed field α_{imp} increases with decreasing values of B_0 .

The test-field method reveals that on branches X, Y and YZ the α_{yy} component is nearly independent of B_0 , and always larger than the α_{xx} component. However, on branch Z and for $R_m \mathbf{B}_0^2 / B_{\text{eq}}^2 < 1$ we find that $\alpha_{xx} = \alpha_{yy}$ and only weakly suppressed.

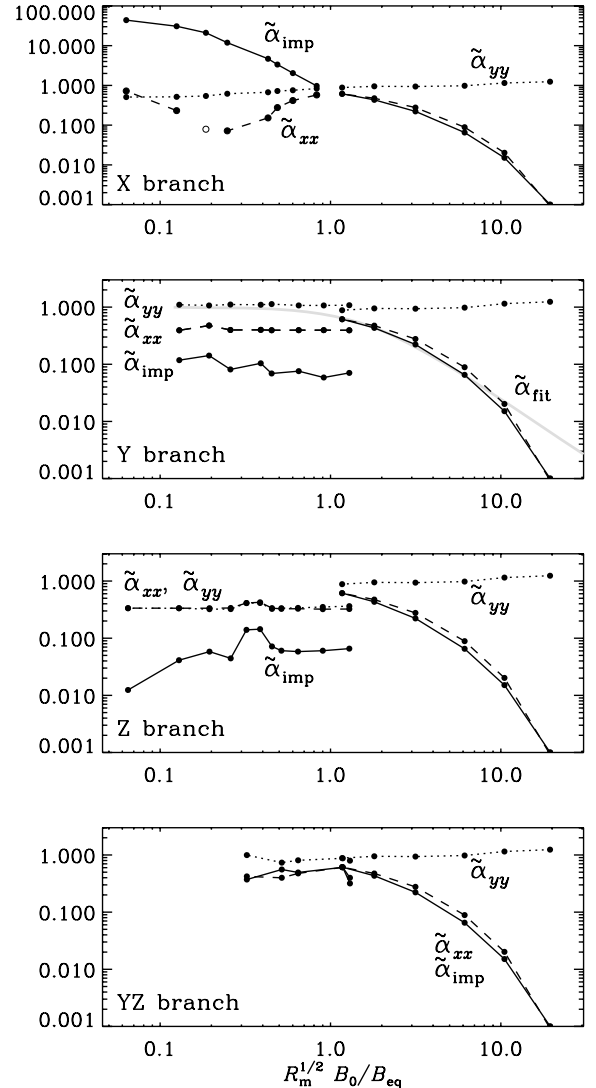


Figure 3. Volume-averaged values of α_{imp} , α_{xx} and α_{yy} . A tilde indicates that the values are normalized by α_0 , i.e. $\tilde{\alpha}_{\text{imp}} = \alpha_{\text{imp}} / \alpha_0$ (solid line), $\tilde{\alpha}_{xx} = \langle \alpha_{xx} \rangle / \alpha_0$ (dashed line), $\tilde{\alpha}_{yy} = \langle \alpha_{yy} \rangle / \alpha_0$ (dotted line) and $\tilde{\alpha}_{\text{fit}} = \alpha_{\text{fit}} / \alpha_0$ (thick grey line, but only shown in the second panel). The two open symbols in the top panel indicate that the values of α_{xx} / α_0 are negative.

A comment regarding the discontinuities in Fig. 3 near $R_m \mathbf{B}_0^2 / B_{\text{eq}}^2 = 1$ is here in order. The systems considered here are in saturated states. To the left of the discontinuities the system has a saturated meso-scale dynamo, while to the right there is none.

Intermediate states are simply not possible. Hence, the discontinuities are caused by the effects of the meso-scale magnetic fields on u_{rms} and thus on R_m .

3.2 Relation to α_1 and α_2

In the following we will try to interpret the results presented above in terms of equation (11) and determine α_1 and α_2 for the different branches. For small values of B_0 , a magnetic field with $k = k_1$ and hence a finite planar average can develop. Compared with the large-scale field B_0 , we refer to this dynamo-generated field as meso-scale magnetic field. As demonstrated in Brandenburg (2001), three types of such mean fields are possible in the final saturated state. These fields correspond to Beltrami fields of the form

$$\frac{\overline{\mathbf{B}}^{(x)}}{B_1} = \begin{pmatrix} 0 \\ c_x \\ s_x \end{pmatrix}, \quad \frac{\overline{\mathbf{B}}^{(y)}}{B_1} = \begin{pmatrix} s_y \\ 0 \\ c_y \end{pmatrix}, \quad \frac{\overline{\mathbf{B}}^{(z)}}{B_1} = \begin{pmatrix} c_z \\ s_z \\ 0 \end{pmatrix}, \quad (16)$$

where $c_\xi = \cos(k_1\xi + \phi)$ and $s_\xi = \sin(k_1\xi + \phi)$ denote cosine and sine functions as functions of $\xi = x, y$ or z , with an arbitrary phase shift ϕ .¹ The precise value of B_1 emerges as a result of the simulation, but based on simulations in a periodic domain (Brandenburg 2001) we know that B_1/B_{eq} should be about $(k_f/k_1)^{1/2}$ times the equipartition value. This is also confirmed by the present calculations.

Let us now discuss separately the different branches. As can be seen from Fig. 4, the weak-field regime is characterized by the presence of meso-scale magnetic fields that vary either in the x direction (the X branch), the y direction (Y branch), the z direction (Z branch) or in both the y and z directions (YZ branch).

In order to get some idea about the values α_1 and α_2 on the various branches, we consider two limiting cases. For strong imposed fields, $\beta \rightarrow \infty$, the results lie formally on the YZ branch, because such a field has only very little variation in the x direction. However, $(\hat{B}_i \hat{B}_j)$ will be dominated only by the uniform field in the x direction, so we have $\epsilon_x = 1$ and $\epsilon_y = 0$; see Section 2.3. This means that $\tilde{\alpha}_{\text{imp}} = \tilde{\alpha}_{xx} = \tilde{\alpha}_1 + \tilde{\alpha}_2$ and $\tilde{\alpha}_{yy} = \tilde{\alpha}_1$, so we can calculate

$$\tilde{\alpha}_1 = \tilde{\alpha}_{yy}, \quad \tilde{\alpha}_2 = \tilde{\alpha}_{\text{imp}} - \tilde{\alpha}_{yy}, \quad (17)$$

where a tilde indicates normalization by α_0 . For weak imposed fields, $\beta \rightarrow 0$, we can calculate $\tilde{\alpha}_1$ and $\tilde{\alpha}_2$ on the X branch by using the relations

$$\tilde{\alpha}_{xx} = \tilde{\alpha}_1, \quad (18)$$

$$\tilde{\alpha}_{yy} = \tilde{\alpha}_1 + \frac{1}{2}\tilde{\alpha}_2, \quad (19)$$

$$\tilde{\alpha}_{\text{imp}} = \tilde{\alpha}_1 + \tilde{\alpha}_2. \quad (20)$$

However, on the X branch $\tilde{\alpha}_{xx}$ is ill determined, as seen in Fig. 3 and discussed in Section 4.1. Therefore, we use only equations (19) and (20) to calculate

$$\tilde{\alpha}_1 = 2\tilde{\alpha}_{yy} - \tilde{\alpha}_{\text{imp}}, \quad \tilde{\alpha}_2 = 2\tilde{\alpha}_{\text{imp}} - 2\tilde{\alpha}_{yy}. \quad (21)$$

For the Y, Z and YZ branches, on the other hand, these relations have to be substituted by

$$\tilde{\alpha}_1 = 2\tilde{\alpha}_{xx} - \tilde{\alpha}_{\text{imp}}, \quad \tilde{\alpha}_2 = 2\tilde{\alpha}_{\text{imp}} - 2\tilde{\alpha}_{xx}. \quad (22)$$

¹ Unlike the case considered by Brandenburg et al. (2008b), here the test field has $k = 0$, and there is no relative phase to be considered.

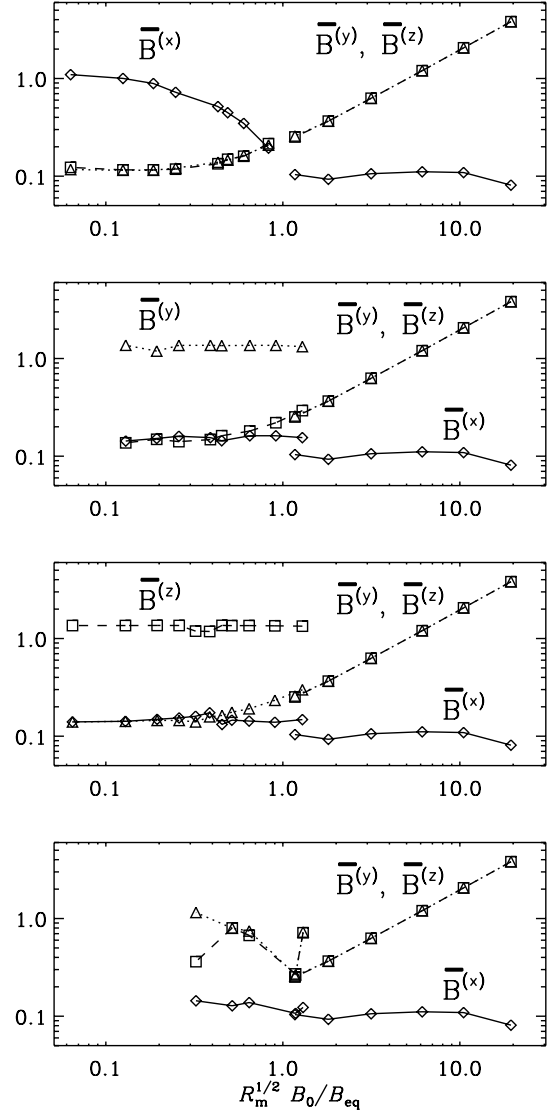


Figure 4. Root-mean-square values of the mean magnetic fields as functions of the imposed field for turbulence with $R_m = 26$ for the X, Y, Z and YZ branches in the same order as in Fig. 3. Diamonds, triangles and squares denote $\overline{\mathbf{B}}^{(x)}$, $\overline{\mathbf{B}}^{(y)}$ and $\overline{\mathbf{B}}^{(z)}$, respectively.

The resulting values of $\tilde{\alpha}_1$ and $\tilde{\alpha}_2$ are plotted in Fig. 5 for each of the four branches. On the Y branch one can, as a test, also use the independent relation $\tilde{\alpha}_1 = \tilde{\alpha}_{yy}$. The resulting values are about 50 per cent larger than the values shown in Fig. 5, suggesting that there could be additional contributions in the simplified relation $\tilde{\alpha}_{yy} = \tilde{\alpha}_1$. On the Z branch, of course, $\tilde{\alpha}_{xx} = \tilde{\alpha}_{yy}$, so here too we have to use the equations (22).

In all cases we find that $\tilde{\alpha}$ is quenched by $\tilde{\alpha}_1$ and $\tilde{\alpha}_2$ having opposite signs and their moduli approaching each other. This is particularly clear in the case of strong fields where $\tilde{\alpha}_1$ and $-\tilde{\alpha}_2$ become indistinguishable, while each of them is still increasing. We note that the turbulence itself is not strongly affected (Brandenburg & Subramanian 2005a). On the Y and Z branches both $\tilde{\alpha}_1$ and $\tilde{\alpha}_2$ are of order unity, but on the X branch they can reach rather large values when the imposed field is weak. The behaviour on the YZ branch is somewhat unsystematic, suggesting that this branch is really just the result of a long-term transient, as was already found in the absence of an imposed field (Brandenburg 2001). However, we decided not

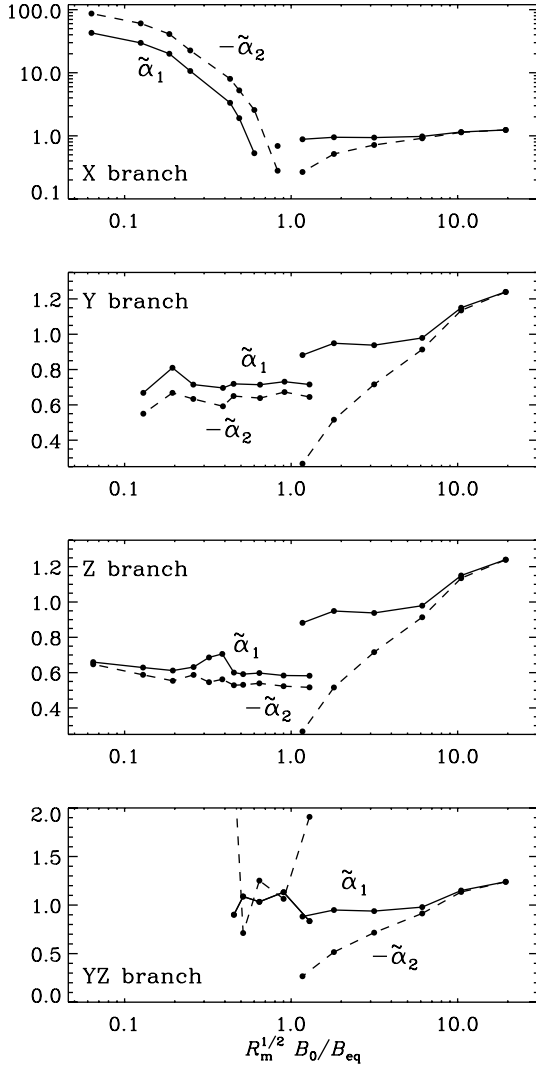


Figure 5. Dependence of α_1 and α_2 on B_0 for the X, Y, Z and YZ branches in the same order as in Fig. 3.

to discard this branch, because it is likely that transient solutions on this branch may become even more long-lived as the magnetic Reynolds number is increased further.

3.3 Enhancement of α_{imp} in the field-aligned case

The suppression of $\alpha = \alpha_1 + \alpha_2$ by the magnetic field is not surprising. What is unexpected, however, is the dramatic enhancement of both α_1 and $-\alpha_2$ for weak imposed fields and equipartition-strength meso-scale fields that vary in the x direction (the field-aligned case or X branch). In this case the interactions of the current density associated with the Beltrami field and the imposed field generate a force varying along x , perpendicular to the components of the meso-scale Beltrami field. This generates a meso-scale velocity that in turn damps the Beltrami field, resulting in the slower rise in $\overline{\mathbf{B}}^{(x)}$ as B_0/B_{eq} is decreased. Further, the cross-product of the meso-scale velocity field with the Beltrami field generates a large-scale electromotive force in the x direction. This is seen both in α_{imp} and in α_{xx} . A rough estimate of this electromotive force can be obtained

by considering the fields

$$\mathbf{B}_0 = \begin{pmatrix} B_0 \\ 0 \\ 0 \end{pmatrix}, \quad \mathbf{B}_1 = B_1 \begin{pmatrix} 0 \\ \cos kx \\ \sin kx \end{pmatrix}, \quad (23)$$

so that $\mu_0 \mathbf{J}_1 = -k \mathbf{B}_1$, where subscript 1 denotes meso-scale fields. The meso-scale current density and the imposed field will generate a meso-scale Lorentz force which will drive a meso-scale velocity field \mathbf{U}_1 . We estimate \mathbf{U}_1 by balancing

$$\mathbf{J}_1 \times \mathbf{B}_0 / \rho + \nu_t \nabla^2 \mathbf{U}_1 \approx 0, \quad (24)$$

where ν_t is the turbulent viscosity. We therefore expect that \mathbf{U}_1 will saturate for

$$\mathbf{U}_1 = \frac{B_0 B_1 / \rho \mu_0}{\nu_t k} \begin{pmatrix} 0 \\ \sin kx \\ -\cos kx \end{pmatrix}. \quad (25)$$

This velocity field will generate an \mathcal{E}_0 parallel to \mathbf{B}_0 in conjunction with \mathbf{B}_1 :

$$\mathcal{E}_0 \equiv \langle \mathbf{U}_1 \times \mathbf{B}_1 \rangle = \alpha_{\text{meso}} \mathbf{B}_0, \quad (26)$$

with $\alpha_{\text{meso}} = B_1^2 / (\rho \mu_0 \nu_t k)$. We then expect the total α_{imp} to be

$$\alpha_{\text{imp}} = \alpha + \frac{B_1^2 / \rho \mu_0}{\nu_t k}. \quad (27)$$

Normalizing by $\alpha_0 = -u_{\text{rms}}/3$ and assuming $\nu_t \approx u_{\text{rms}}/3k_f$ we find for small imposed field and a meso-scale dynamo that varies along x :

$$\frac{\alpha_{\text{imp}}}{\alpha_0} \approx 1 + 9 \frac{k_f}{k_1} \left(\frac{B_1}{B_{\text{eq}}} \right)^2. \quad (28)$$

Given that $k_f/k_1 = 3$ and noting that B_1/B_{eq} reaches values up to 1.2, we find that $\alpha_{\text{imp}}/\alpha_0 \approx 40$, which is still somewhat below the actual value of 53; see the top panel of Fig. 3. The remaining discrepancy may be explicable by recalling that the actual value of ν_t may well be reduced due to the presence of an equipartition-strength magnetic field.

3.4 Comment on wavenumber dependence

In previous work on the test-field method we used test fields with wavenumbers different from zero. It turned out that in the kinematic regime, α is proportional to $1/[1 + a(k/k_f)^2]$, where $a = 0.5, \dots, 1$ (Brandenburg et al. 2008a; Mitra et al. 2009). It was shown that the variation of α with k represents non-locality in space. In order to get some idea about the dependence of α_{xx} and α_{yy} on k in the present case we compare in Table 3 the results for $k = k_0$ with those for $k = 0$. It turns out that both values decrease by 30 per cent on the X branch, and increase by less than 10 per cent on the Z branch.

Table 3. Examples of the dependence of $\tilde{\alpha}_{xx}$ and $\tilde{\alpha}_{yy}$ on the wavenumber k of the test field. Note that the field strength is different in both cases.

Branch	k/k_0	$\tilde{\alpha}_{xx}$	$\tilde{\alpha}_{yy}$	$R_m^{1/2} B_0 / B_{\text{eq}}$
X	0	0.72 ± 0.14	0.51 ± 0.16	0.06
	1	0.61 ± 0.02	0.37 ± 0.01	0.06
Z	0	0.34 ± 0.02	0.32 ± 0.02	0.2
	1	0.35 ± 0.01	0.35 ± 0.02	0.2

The k dependence for the Z branch is minor, although one would have expected a small decrease rather than an increase. Nevertheless, within error bars, this result is possibly still compatible with the dependence in the kinematic case. For the X branch the error bars for $k = 0$ are larger. This is because of the strong interaction between the imposed uniform field and a Beltrami field varying along the same direction, as discussed in Section 3.3. It is therefore not clear whether the k dependence is here significant and how to interpret it.

4 RESETTING THE FLUCTUATIONS

4.1 Effectiveness of resetting the fields

The evolution equations used both in the imposed-field method and in the test-field method allow for dynamo action. This led Ossendrijver et al. (2002) and Käpylä et al. (2006) to the technique of resetting the resulting magnetic field in regular intervals. This method is now also routinely used in the test-field approach (Sur et al. 2008), and we have also used it throughout this work. The lack of resetting the magnetic field may also be the main reason for the rather low values of α found in the recent work of Hughes & Proctor (2009); see the corresponding discussion in Käpylä et al. (2009b).

In this section we employ the method of resetting \mathbf{B} to obtain better estimates for α for weak imposed fields, and to compare this with results from the test-field method. The result is shown in Fig. 6 where we show the dependence of α_{imp} on B_0 and on the reset interval Δt . We note that, in units of the turnover time, the reset interval $\Delta t u_{\text{rms}} k_f$ has a weak dependence both on B_0 and Δt ,

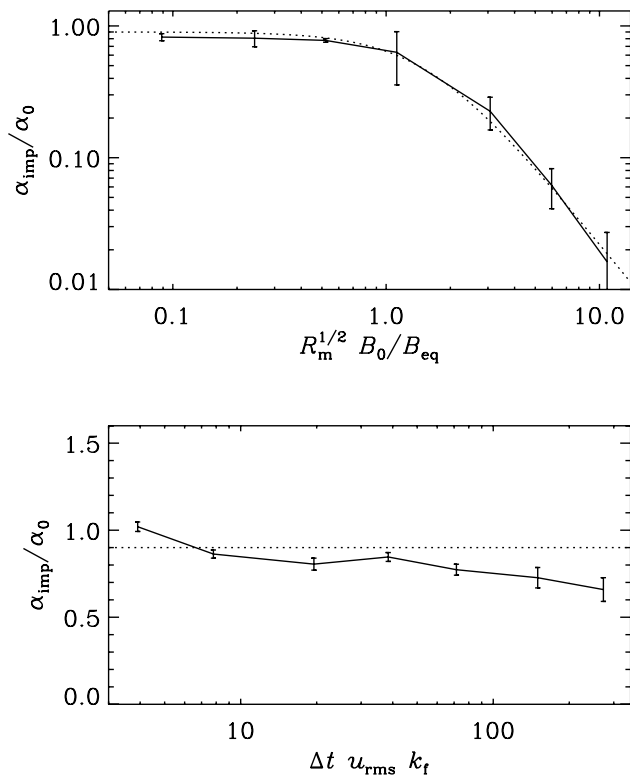


Figure 6. Dependence of α_{imp} (solid lines) and α_{fit} (dotted lines) on the imposed field strength with fixed reset time $\Delta t u_{\text{rms}} k_f = 50, \dots, 70$ (upper panel) and the dependence of α_{imp} on the reset time for $R_m^{1/2} B_0/B_{\text{eq}} = 0.1$ (lower panel). In all cases we have $R_m \approx 30$.

Table 4. Comparison of the results for $\tilde{\alpha}_{xx}$ and $\tilde{\alpha}_{yy}$ for two different reset times Δt for the examples of the X and Z branches with $R_m^{1/2} B_0/B_{\text{eq}} = 0.2$. The reset time is normalized by the inverse turnover time $(u_{\text{rms}} k_f)^{-1}$.

Branch	$\Delta t u_{\text{rms}} k_f$	$\tilde{\alpha}_{xx}$	$\tilde{\alpha}_{yy}$
X	25	-0.08 ± 0.13	0.54 ± 0.02
	50	-0.98 ± 0.09	0.70 ± 0.04
Z	25	0.34 ± 0.02	0.32 ± 0.02
	50	0.32 ± 0.01	0.33 ± 0.03

because small values of B_0 and Δt quench u_{rms} only weakly. The resetting technique has eliminated the branching for weak fields. For weak fields we find that the value of α_{imp} is slightly below α_0 , but this is partly because for finite scale separation there is an additional factor $(1 + k_f^2/k_1^2)^{-1} \approx 0.9$ (Brandenburg et al. 2008a). The actual value of α_{imp} is somewhat smaller still, which may be ascribed to other systematic effects.

It turns out that over a wide range of reset intervals the resulting values of α_{imp} are not dependent in a systematic way on the reset interval (see also Mitra et al. 2009), although it is clear that the error bars increase for larger values of Δt . The same is true for the values of α_{xx} and α_{yy} obtained using the test-field method, except for the case of weak fields on the X branch where the values of α_{xx} are ill determined; see Table 4, where we compare the values of α_{xx} and α_{yy} for two different reset times in the case where α_{xx} is found to change sign ($R_m^{1/2} B_0/B_{\text{eq}} \approx 0.2$). The increasing fluctuations for longer reset intervals occur as the system exits the kinematic regime. It might therefore be possible to find indicators of when the kinematic regime has been exited and resetting becomes necessary. However, we have not pursued this further in this work.

For even larger values of Δt there is enough time for the meso-scale magnetic field to develop. An example is shown in Fig. 7 where 18 intervals of length $\Delta t u_{\text{rms}} k_f = 270$ are shown. For half of these intervals the wavevector of the Beltrami field begins to develop in the x direction, so α_{imp} is heading toward the X branch. In the other half of these cases the magnetic field is weak and α_{imp} lies on one of the other branches. None of these cases reproduce the correct kinematic value of α , because we are not really considering a kinematic problem in this case. This underlines the importance of choosing reset intervals that are not too long.

Our results support the hypothesis that the precise value of the reset time interval is not critical except for the field-aligned case

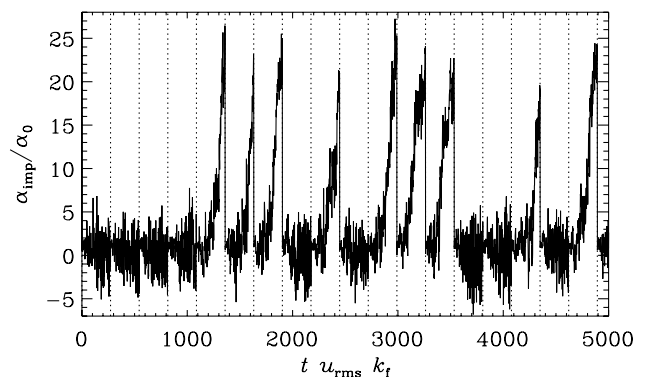


Figure 7. Time series of α_{imp} for $\Delta t u_{\text{rms}} k_f = 270$ with $R_m^{1/2} B_0/B_{\text{eq}} = 0.1$. The reset intervals are indicated by dotted vertical lines. In all cases we have $R_m \approx 30$.

where the diagonal components of the α_{ij} tensor are large and quite uncertain, as indicated also by the large error bars. The sign change found for α_{xx} at low or intermediate field strengths might therefore not be real.

4.2 Time averaging in the test-field method

We have already demonstrated that the length of the reset interval is not critical for the value of α , but longer reset times tend to lead to larger errors. In the present section we demonstrate this for the test-field method using the idealized case where the turbulent flow velocity is replaced by simple stationary flow given by the equation

$$\mathbf{U} = k_f \varphi \hat{z} + \nabla \times (\varphi \hat{z}), \quad (29)$$

with

$$\varphi = \varphi(x, y) = u_0 \cos k_0 x \cos k_0 y, \quad (30)$$

which is known as the Roberts flow.

When the magnetic Reynolds number exceeds a certain critical value of around 60, some kind of dynamo action of \mathbf{b}^q commences. This type of dynamo is often referred to as small-scale dynamo action (Brandenburg et al. 2008b; Sur et al. 2008; Cattaneo & Hughes 2009), but this name may not always be accurate. In the case of the Roberts flow there would be no such dynamo action if the wavenumber of the test field is zero, $k = 0$, as assumed here. However, for $k = k_0$, for example, dynamo action for the test-field equation is possible. The test fields are therefore chosen to be

$$\frac{\overline{\mathbf{B}}^1}{B} = \begin{pmatrix} \cos kz \\ 0 \\ 0 \end{pmatrix}, \quad \frac{\overline{\mathbf{B}}^2}{B} = \begin{pmatrix} \sin kz \\ 0 \\ 0 \end{pmatrix}, \quad (31)$$

$$\frac{\overline{\mathbf{B}}^3}{B} = \begin{pmatrix} 0 \\ \cos kz \\ 0 \end{pmatrix}, \quad \frac{\overline{\mathbf{B}}^4}{B} = \begin{pmatrix} 0 \\ \sin kz \\ 0 \end{pmatrix}, \quad (32)$$

see Sur et al. (2008). Since now the mean fields are also functions of z , the term $\mathbf{u} \times \mathbf{b}^q$ cannot be omitted in equation (8).

As stressed by Brandenburg et al. (2008a), in the expression for the electromotive force there is in general also a contribution \mathcal{E}_0 that is independent of the mean field. Given that test fields $\overline{\mathbf{B}}^q$ are independent of time, we have

$$\overline{\mathcal{E}}^q(z, t) = \overline{\mathcal{E}}_0^q(z, t) + \alpha(z) \overline{\mathbf{B}}^q(z) - \eta_t(z) \mu_0 \overline{\mathbf{J}}^q(z), \quad (33)$$

where overbars denote xy averages (not volume averages), so there is also a term $\eta_t \mu_0 \overline{\mathbf{J}}^q$, where η_t is the turbulent magnetic diffusivity. We have assumed that α and η_t are independent of time, and in this case they are also independent of z . The $\overline{\mathcal{E}}_0^q(z, t)$ term can be eliminated by averaging over time, i.e. $\langle \overline{\mathcal{E}}_0^q \rangle = 0$, so

$$\langle \overline{\mathcal{E}}^q \rangle = \alpha \overline{\mathbf{B}}^q - \eta_t \mu_0 \overline{\mathbf{J}}^q. \quad (34)$$

In Fig. 8 we show the evolution of α for the Roberts flow with $R_m = 65$ and 55. In the case with $R_m = 65$ there are exponentially growing oscillations corresponding to a wave travelling in the z direction. In general such fields can be a superposition of waves travelling in the positive and negative z directions. It is seen quite clearly that the running time average is stable and well defined. The results for $R_m = 65$ and 55 are close together ($\alpha/\alpha_0 = 0.096$ and 0.090, respectively), suggesting continuity across the point where dynamo action sets in. This supports the notion that averaging over time is a meaningful procedure.

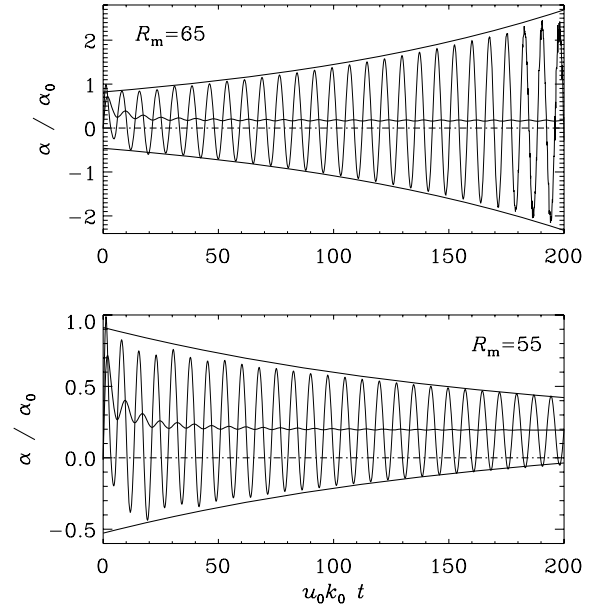


Figure 8. Plot of the instantaneous α for $R_m = 65$ (upper panel) and $R_m = 55$ (lower panel). In both cases running means are overlotted and converge to nearly the same value of about -0.096 in the upper panel and -0.090 in the lower one. The envelope functions are well described by exponentials and are also overlotted. Note, however, the different scales on the ordinate of both panels. The dash-dotted line shows the zero level.

5 CONCLUSIONS

The present simulations have shown that the imposed-field method leads to a number of interesting and unexpected results. For imposed fields exceeding the value $R_m^{-1/2} B_{\text{eq}}$ one recovers the catastrophic quenching formula of Vainshtein & Cattaneo (1992); see equation (15). We emphasize once more, however, that this formula is only valid for completely uniform large-scale fields in a triply periodic domain. This is clearly artificial, but it provides an important benchmark.

A number of surprising results have been found for weaker fields of less than $R_m^{-1/2} B_{\text{eq}}$. In virtually none of those cases does the imposed-field method recover the kinematic value of α . Instead, α_{imp} can attain strongly suppressed values, but it can actually also attain strongly enhanced values. This is caused by the unavoidable emergence of meso-scale dynamo action. In principle, such meso-scale dynamo action could have been suppressed by restricting oneself to scale-separation ratios, k_f/k_1 , of less than 2 or so. This was done, for example, in some of the runs of Brandenburg & Subramanian (2005a). In the present case of a triply periodic box, four different magnetic field configurations can emerge. The first three correspond to Beltrami fields, where the wavevector points in one of the three coordinate directions. The fourth possibility is also a Beltrami field, but one that varies diagonally in a direction perpendicular to the direction of the imposed field. The latter was found to be unstable in the absence of an imposed field, but they can be long-lived in the present case of an imposed field.

In this paper, we have used the term meso-scale fields to refer to the Beltrami fields naturally generated by the helicity-driven dynamo in our system. A more general definition of meso-scale fields would encompass all fields that break isotropy, average to zero, and yet do not time-average to zero. In the absence of such fields, mean-field theory can be applied in a straightforward manner. This is indeed the case that one is normally interested in. However, when

such meso-scale fields exist, they must be understood for determining turbulent transport coefficients, because those coefficients apply then to the particular case of saturated meso-scale fields.

The results obtained with the imposed-field method reflect correctly the circumstances in the non-linear case where the α effect is suppressed by dynamo-generated meso-scale magnetic fields whose scale is smaller than that of the imposed field, but comparable to the scale of the domain. Especially in the case of closed or periodic domains the resulting α is catastrophically quenched, which is now well understood (Blackman & Brandenburg 2002; Field & Blackman 2002). This effect is particularly strong in the case where one considers volume averages, and thus ignores the effects of turbulent magnetic diffusion. With magnetic diffusion included, both α and η_t have only a mild dependence on R_m (Brandenburg et al. 2008b). However, astrophysical dynamos are expected to operate in a regime where magnetic helicity fluxes alleviate catastrophic quenching; see Brandenburg & Subramanian (2005b) for a review.

Determining the nature of the dynamo mechanism is an important part in the analysis of a successful simulation showing large-scale field generation. Our present analysis shows that meaningful results for α can be obtained using either the imposed-field or the test-field methods provided the departure of the magnetic field from \mathbf{B}_0 is reset to zero to eliminate the effects of dynamo-generated meso-scale magnetic fields. Conversely, if such fields are not eliminated, the results can still be meaningful, as demonstrated here, but they need to be interpreted correspondingly and bear little relation to the imposed field. On the other hand, for strong imposed magnetic fields ($R_m \mathbf{B}_0^2 / B_{\text{eq}}^2 > 1$), meso-scale magnetic fields tend not to grow, so the resetting procedure is then neither necessary nor would it make much of a difference when the test-field method is used. However, when the imposed-field method is used, the resetting of the actual field reduces the quenching of u_{rms} . This affects the normalizations of B_0 and α_{ij} with B_{eq} and α_0 , respectively, because both are proportional to u_{rms}^2 .

Throughout this paper we have considered relatively moderate values of R_m , but we computed a large number of different simulations. In the beginning of this study we started with larger values of R_m and found that the resulting α_{imp} seemed inconsistent. In hindsight it is clear what happened: the few cases that we had in the beginning were all scattered around different branches. Only later, by performing a large number of simulations at smaller values of R_m it became clear that there are indeed different branches. This highlights the importance of studying not just one or a few models of large R_m , but rather a larger systematic set of intermediate cases of moderate R_m where it is possible to understand in detail what is going on. It will be important to continue exploring the regime of larger R_m , and we hope that the new understanding that emerged from studying cases of moderate R_m proves useful in this connection. According to the results available so far, we can say that for larger values of R_m the turbulent transport coefficients are only weakly affected (see Brandenburg et al. 2008b, for $R_m \leq 600$) for fields of equipartition strength, or not affected at all (Sur et al. 2008, for $R_m \leq 220$) if the field is in the kinematic limit.

ACKNOWLEDGMENTS

We thank the referee for making a number of constructive remarks on the paper. We acknowledge the use of computing time at the

Center for Parallel Computers at the Royal Institute of Technology in Sweden and CSC – IT Center for Science in Espoo, Finland. This work was supported in part by the European Research Council under the AstroDyn Research Project 227952 (FDS), the Academy of Finland grant 121431 (PJK) and the Swedish Research Council grant 621-2007-4064 (AB).

REFERENCES

- Blackman E. G., Brandenburg A., 2002, *ApJ*, 579, 359
 Brandenburg A., 2001, *ApJ*, 550, 824
 Brandenburg A., 2009, *ApJ*, 697, 1206
 Brandenburg A., Subramanian K., 2005a, *A&A*, 439, 835
 Brandenburg A., Subramanian K., 2005b, *Phys. Rep.*, 417, 1
 Brandenburg A., Nordlund A., Pulkkinen P., Stein R. F., Tuominen I., 1990, *A&A*, 232, 277
 Brandenburg A., Rädler K.-H., Schrunner M., 2008a, *A&A*, 482, 739
 Brandenburg A., Rädler K.-H., Rheinhardt M., Subramanian K., 2008b, *ApJ*, 687, L49
 Brown B. P., Browning M. K., Brun A. S., Miesch M. S., Nelson N. J., Toomre J., 2007, in Stancliffe R. J., Houdek G., Martin R. G., Tout C. A., eds, *AIP Conf. Proc.* 948. *Unsolved Problems in Stellar Physics*. Am. Inst. Phys., New York, p. 271
 Browning M. K., Miesch M. S., Brun A. S., Toomre J., 2006, *ApJ*, 648, L157
 Cattaneo F., Hughes D. W., 1996, *Phys. Rev. E*, 54, R4532
 Cattaneo F., Hughes D. W., 2006, *J. Fluid Mech.*, 553, 401
 Cattaneo F., Hughes D. W., 2009, *MNRAS*, 395, L48
 Field G. B., Blackman E. G., 2002, *ApJ*, 572, 685
 Gruzinov A. V., Diamond P. H., 1994, *Phys. Rev. Lett.*, 72, 1651
 Haugen N. E. L., Brandenburg A., Dobler W., 2004, *Phys. Rev. E*, 70, 016308
 Hughes D. W., Cattaneo F., 2008, *J. Fluid Mech.*, 594, 445
 Hughes D. W., Proctor M. R. E., 2009, *Phys. Rev. Lett.*, 102, 044501
 Käpylä P. J., Korpi M. J., Ossendrijver M., Stix M., 2006, *A&A*, 455, 401
 Käpylä P. J., Korpi M. J., Brandenburg A., 2008, *A&A*, 491, 353
 Käpylä P. J., Korpi M. J., Brandenburg A., 2009a, *ApJ*, 697, 1153
 Käpylä P. J., Korpi M. J., Brandenburg A., 2009b, *A&A*, 500, 633
 Krause F., Rädler K.-H., 1980, *Mean-Field Magnetohydrodynamics and Dynamo Theory*. Pergamon Press, Oxford
 Mininni P. D., 2007, *Phys. Rev. E*, 76, 026316
 Mitra D., Käpylä P. J., Tavakol R., Brandenburg A., 2009, *A&A*, 495, 1
 Moffatt H. K., 1978, *Magnetic Field Generation in Electrically Conducting Fluids*. Cambridge Univ. Press, Cambridge
 Ossendrijver M., Stix M., Brandenburg A., Rüdiger G., 2002, *A&A*, 394, 735
 Parker E. N., 1979, *Cosmical Magnetic Fields*. Clarendon Press, Oxford
 Proctor M. R. E., 2007, *MNRAS*, 382, L39
 Rogachevskii I., Kleeorin N., 2003, *Phys. Rev. E*, 68, 036301
 Rogachevskii I., Kleeorin N., 2004, *Phys. Rev. E*, 70, 046310
 Schrunner M., Rädler K.-H., Schmitt D., Rheinhardt M., Christensen U., 2005, *Astron. Nachr.*, 326, 245
 Schrunner M., Rädler K.-H., Schmitt D., Rheinhardt M., Christensen U., 2007, *Geophys. Astrophys. Fluid Dyn.*, 101, 81
 Silant'ev N. A., 2000, *A&A*, 364, 339
 Sokolov D. D., 1997, *Astron. Rep.*, 41, 68
 Sur S., Brandenburg A., Subramanian K., 2008, *MNRAS*, 385, L15
 Tilgner A., Brandenburg A., 2008, *MNRAS*, 391, 1477
 Vainshtein S. I., Cattaneo F., 1992, *ApJ*, 393, 165
 Vishniac E. T., Brandenburg A., 1997, *ApJ*, 475, 263
 Zeldovich Ya. B., 1957, *Sov. Phys. JETP*, 4, 460

This paper has been typeset from a $\text{\TeX}/\text{\LaTeX}$ file prepared by the author.

² This explains why $\Delta t u_{\text{rms}} k_f$ is 70 in Fig. 6 and 50 in Table 4 under otherwise comparable conditions, except that here only the test field is reset and not the actual fluctuating one.